Appendix

Table of content

Appendix Supplementary Figures and Figure legends

Appendix Figure S1

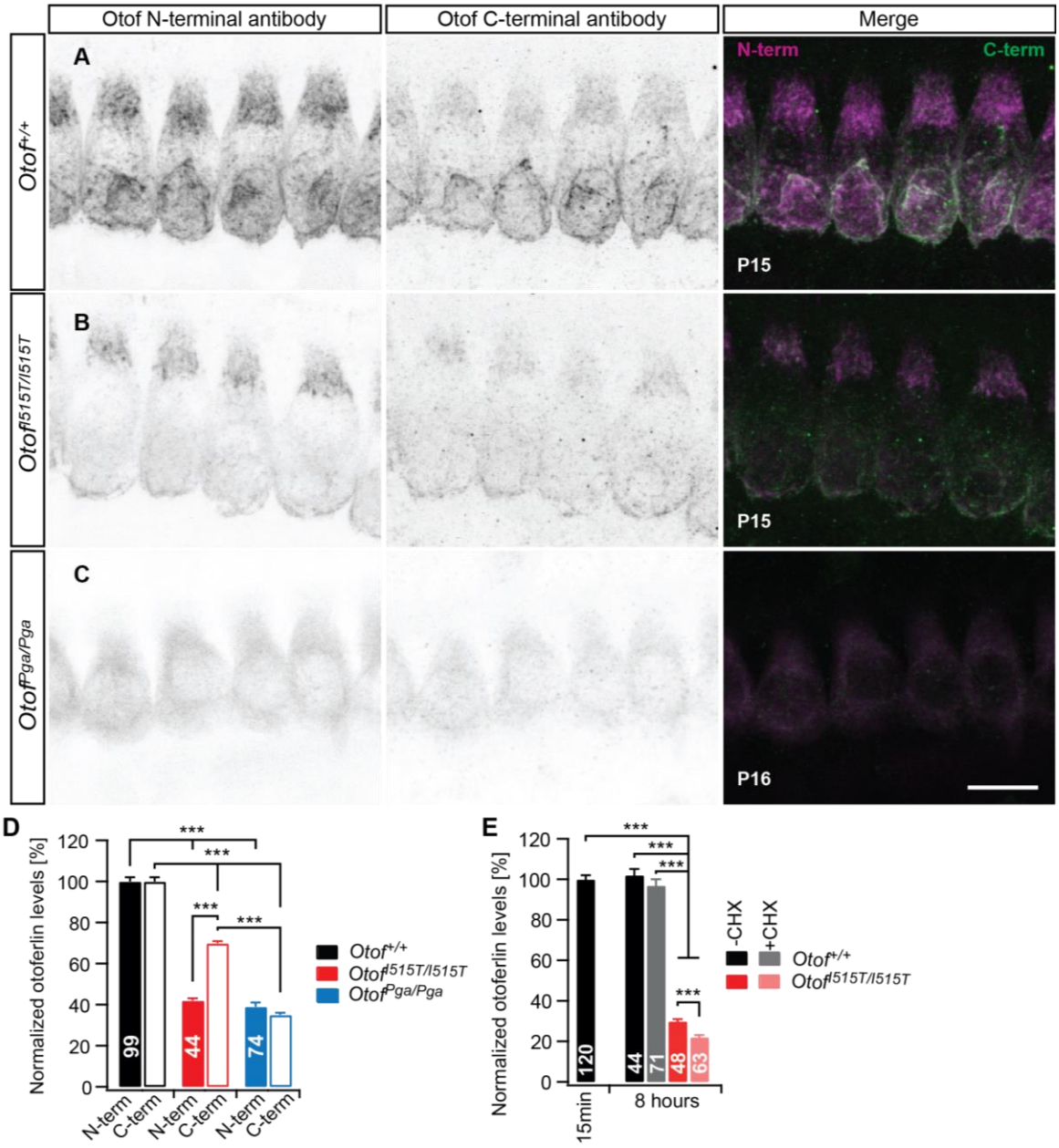

Appendix Figure S1

Lower protein levels of otoferlin in *Otof*$^{I515T/I515T}$ and in *Otof*$^{Pga/Pga}$ IHCs.

A-C, the reduction in cellular otoferlin levels were analyzed with two different anti-otoferlin antibodies: one binding an N-terminal epitope (Abcam, magenta), and one binding a very C-terminal epitope downstream of the transmembrane domain (Synaptic Systems, green). Both antibodies bind to plasma-membrane bound otoferlin in in *Otof*$^{+/+}$ and *Otof*$^{I515T/I515T}$. The N-terminal antibody displays a stronger intracellular staining than the C-terminal antibody, potentially due to binding to incompletely transcribed otoferlin fragments, and/or because the epitope of the C-terminal antibody might be less accessible. Scale bar, 10µm.

D, Quantification of otoferlin levels in P14 IHCs with the N-terminal (solid bars) and the C-terminal (open bars) antibodies both show a reduction in otoferlin levels in mutant IHCs. The stronger reduction in *Otof*$^{I515T/I515T}$ visualized by the N-terminal antibody might reflect a stronger decay in cytoplasmatic otoferlin while otoferlin at the plasma membrane seems better preserved (mean ± SEM, Kruskal-Wallis test).

E, protein biosynthesis was blocked by application of 50µg/ml cycloheximide (CHX) to determine protein degradation in explanted organs of Corti. In contrast to wild type otoferlin, Ile515Thr-otoferlin was significantly degraded in IHCs 8h after stop of protein biosynthesis, providing a potential reason for the chronically lower otoferlin levels in *Otof*$^{I515T/I515T}$ IHCs (mean ± SEM, Kruskal-Wallis test).

Appendix Figure S2

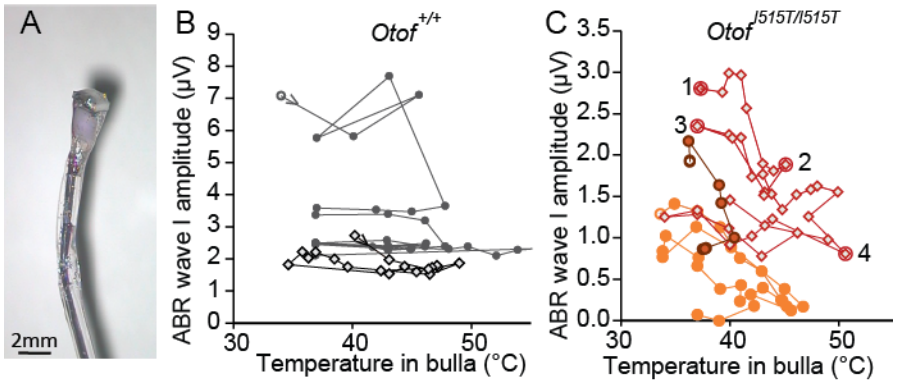

Appendix Figure S2

Temporary and permanent reductions of ABR amplitudes upon local heating

A, Custom-designed heat probe to be placed on the bulla during mouse ABR recordings: a small resistor and a temperature sensor were positioned on a glass capillary and embedded in heat-resistant glue. B, C, In a subset of the experiments partly shown Figure 5 B/C (same colors), ABR amplitudes remained irreversibly low after excessive heating.

Appendix Figure S3

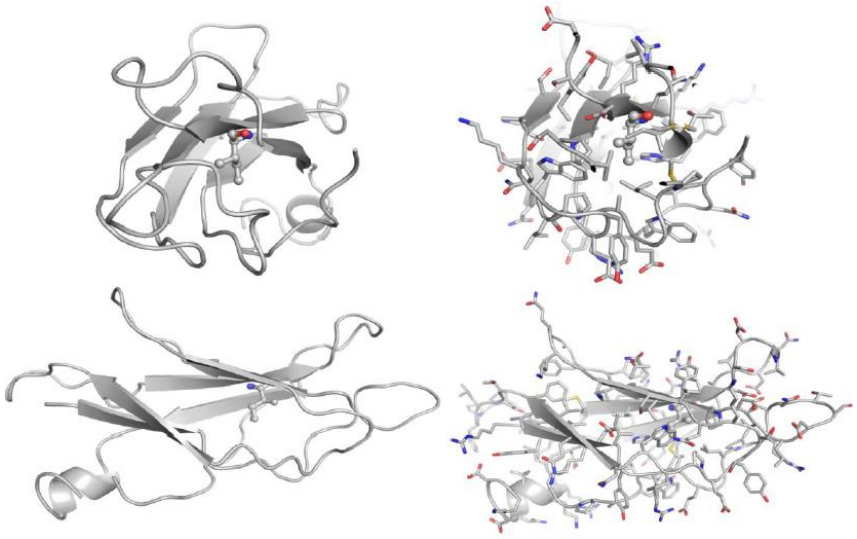

Appendix Figure S3

The residue of isoleucine 515 is predicted to point towards the hydrophobic core of the C_2C domain.

Ile515 is depicted as ball and stick model within the C_2C domain; two different perspectives without (left) and with (right) amino acid side chains. Homology modeling of C_2C domain has been performed with Rosetta (Raman *et al*, 2009) package using the structure of a C_2 domain of a regulating synaptic membrane exocytosis protein 2 (PDB id: 2BWQ) as the template. The template has been identified using HHPRED search server (Söding *et al*, 2005) and shares with the target sequence 24% and 52.6% of sequence identity and similarity, respectively. The hydrophobic core has a strong contribution to the thermal stability of a protein domain due to the aggregation of the non-polar side chains in the interior of the protein. This favors the increase in entropy of the solvent molecules and decreases the conformational flexibility of the folded relative to the unfolded protein. Introducing the Ile515Thr mutation is suggested to result in an unfavorable placement and burial of the polar group in the hydrophobic core of the protein which likely decreases the protein stability. Models and images were kindly provided by Piotr Neumann, University of Goettingen.

Appendix Figure S4

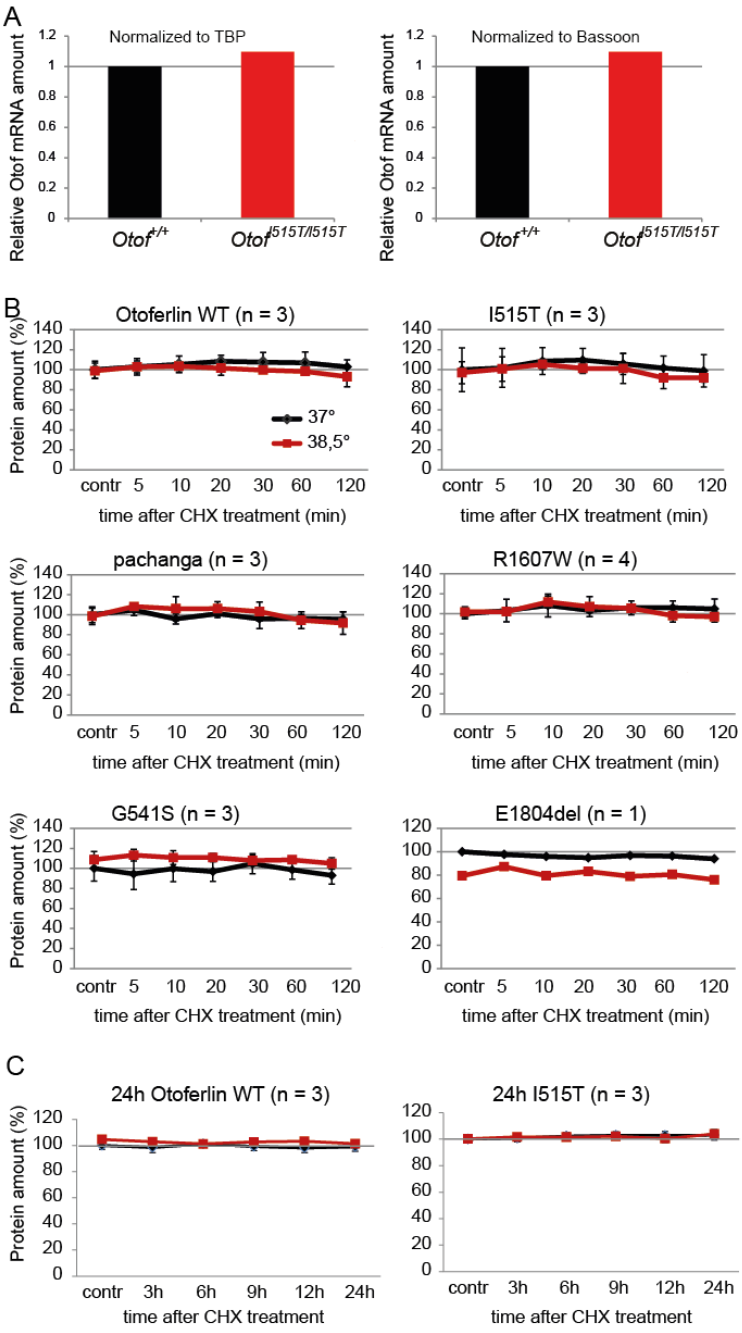

Appendix Figure S4
No differences in mRNA expression levels and no fast degradation of mutated otoferlin in HEK cells.

A, Quantitative PCR reveals no difference in expression levels of otoferlin mRNA in *Otof*$^{I515T/I515T}$ or *Otof*$^{+/+}$ organs of Corti. Otoferlin transcripts were quantified by a taqman based real-time PCR in three cDNA samples from *Otof*$^{+/+}$organs of Corti and two cDNA samples from *Otof*$^{I515T/I515T}$ organs of Corti, prepared as described in Appendix Supplementary Methods. Otoferlin cDNA was normalized either to Tata-binding protein (TBP), which is expressed to a similar level in each cell (left panel), or to bassoon which is expressed in IHCs and spiral ganglion neurons but not in supporting cells or other epithelial cells in the organ of Corti (right panel). The Ile515Thr mutation did not lead to lower otoferlin mRNA levels in *Otof*$^{I515T/I515T}$ organs of Corti.

B, Protein degradation was quantified after expression of otoferlin cDNA and cycloheximide treatment in HEK293T cells (see Appendix Supplementary Methods). Mutations were selected as they were described to cause temperature dependent hearing loss in humans (Marlin *et al*, 2010; Matsunaga *et al*, 2012; Romanos *et al*, 2009; Varga *et al*, 2006; Wang *et al*, 2010). HEK cells were incubated either at 37°C or at 38.5°C, and samples were taken at indicated time points to quantify otoferlin protein levels by means of mass spectrometry (see Appendix Supplementary Methods). N-numbers in the figure indicate biological replicates (charges of transfected HEK cells), while each of these samples was quantified in mass spectrometry in triplicates. Protein amounts were normalized to the control sample at 37°C for each construct (in graphs: normalized mean ± standard deviation). If protein de-stabilization leading to protein degradation would be a major mechanism for the hearing loss, we would expect to see differences in protein stability between mutant and wild-type protein, especially at 38.5°C. However, mutant and wild-type otoferlin protein seem to be stable within two hours under both temperature conditions tested, thereby making it unlikely that fast protein degradation is a major mechanism contributing to deafening at higher temperature. C, Protein amounts within 24h for wild type otoferlin and Ile515Thr-otoferlin indicate no visible degradation in HEK cells during cycloheximide treatment. Nevertheless, we cannot exclude that elevated temperature leads to a fast unfolding of the protein which would not be visible in our experimental setting.

Appendix Figure S5

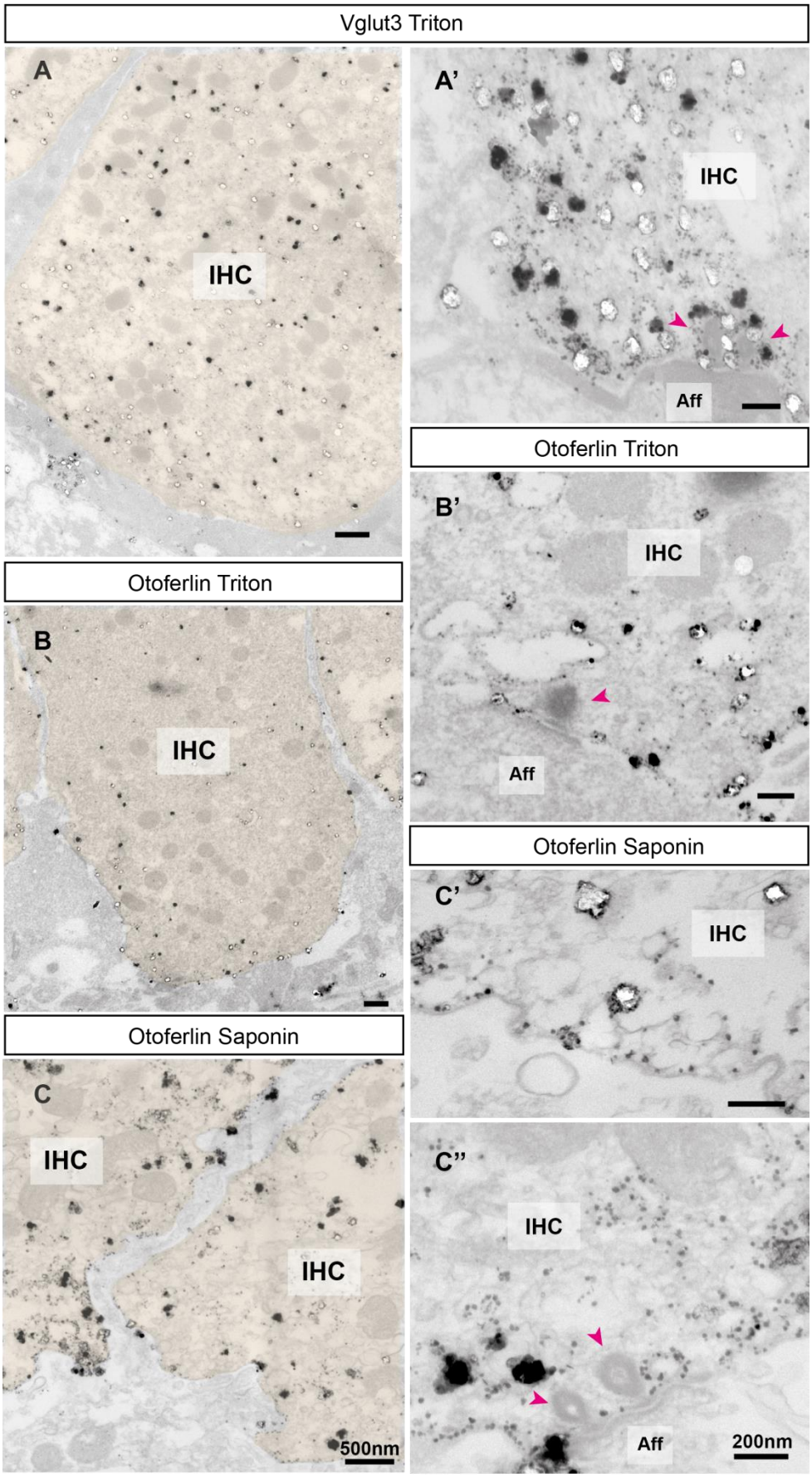

Appendix Figure S5: Pre-embedding immunogold labeling

A-B', Immunogold labelling of IHCs after Triton-X-100 treatment against Vglut3 (A,A') and otoferlin (B,B'). C-C'', Immunogold labelling of IHCs after Saponin treatment. A-C were processed in parallel. In both labelling protocols otoferlin is clearly found in the plasma membrane, whereas Vglut3 staining is only found in the cytoplasm. (Aff) Afferent bouton. Ribbons are indicated with magenta arrowheads, IHCs are highlighted in beige. Scale bars left panel: 500 nm, scale bars right panel: 200 nm.

Appendix Figure S6

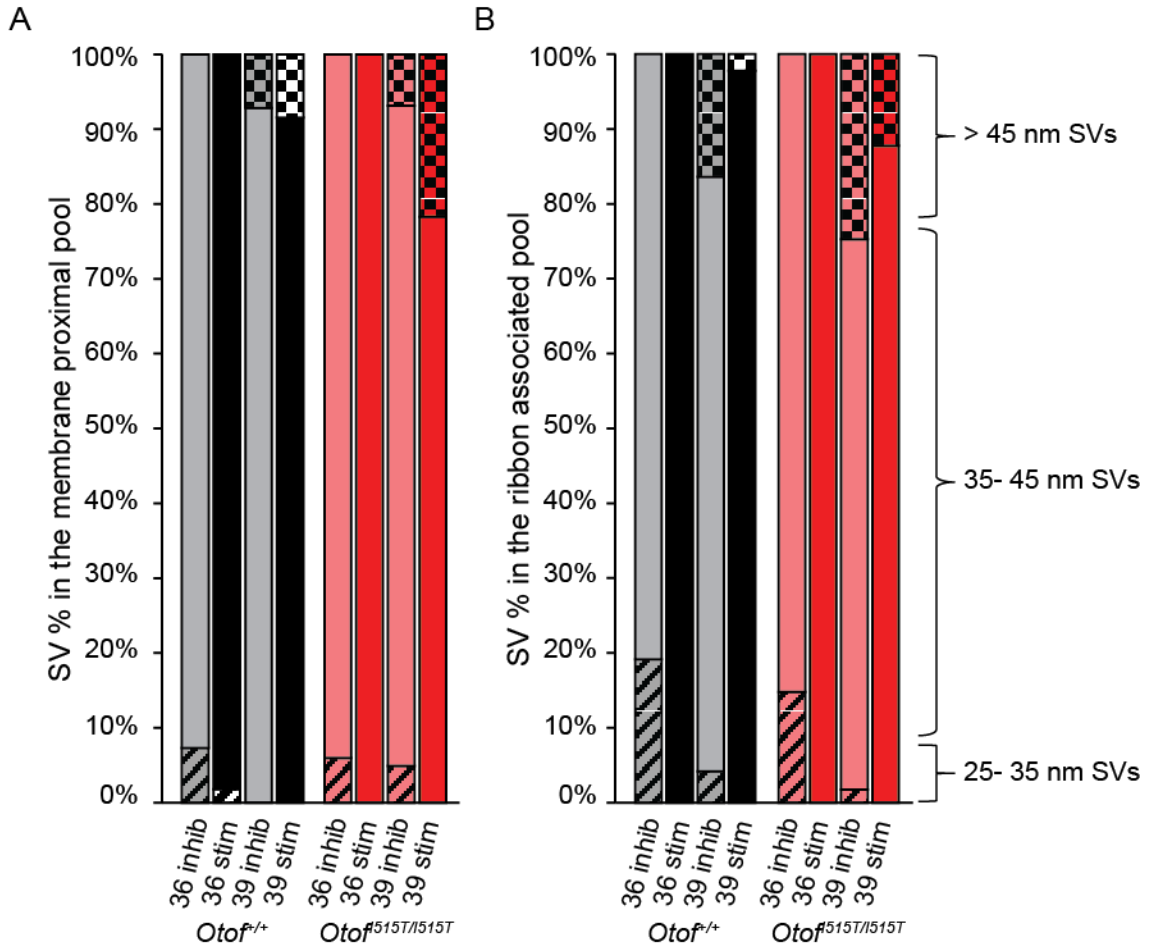

Appendix Figure S6

Electron micrograph parameters for *Otof*$^{I515T/I515T}$ and *Otof*$^{+/+}$ ribbon synapses

A, Size distribution of membrane proximal vesicles for inhibitory and stimulatory conditions at 36°C and 39°C in random sections, indicating that the majority of vesicles were of normal size (35-45 nm diameter). Larger vesicles appeared only at 39°C.

B, Size distribution of ribbon-associated vesicles.

Supplementary Table

Appendix Table S1

Random section analysis of EM

	Conditions	*Otof*$^{+/+}$	n	*Otof*$^{I515T/I515T}$	n	p values
Number of synaptic vesicles in the **ribbon associated pool**	36°C Inhibition	8.6±0.5	36	9.3±0.7	21	p > 0.05 *
	36°C Stimulation	8.8±0.7	25	9.9±0.5	34	p > 0.05 *
	39°C Inhibition	8.9±0.6	24	9.6±0.5	36	p > 0.05 *
	39°C Stimulation	8.4±0.6	27	8.6±0.5	21	p > 0.05 *
Number of synaptic vesicles in the **membrane proximal pool**	36°C Inhibition	2.3±0.1		2.4±0.2		p > 0.05 #
	36°C Stimulation	2.2±0.2		3.5±0.3		p < 0.01 #
	39°C Inhibition	2.3±0.1		2.8±0.1		p > 0.05 #
	39°C Stimulation	2.6±0.2		4±0.3		p <0.05 #
Number of **large**(>45nm) vesicles in the **ribbon associated pool**	36°C Inhibition	0		0		
	36°C Stimulation	0		0		
	39°C Inhibition	1.5±0.2		2.4±0.3		p > 0.05 *
	39°C Stimulation	0.2±0.1		1.04±0.3		p < 0.05 *
Number of **large**(>45nm) vesicles in the **membrane proximal pool**	36°C Inhibition	0		0		
	36°C Stimulation	0		0		
	39°C Inhibition	0.2±0.1		0.2±0.1		p > 0.05 #
	39°C Stimulation	0.2±0.1		0.9±0.3		p < 0.05 #

Data information: P values are calculated by one way ANOVA followed by Tukey's test (*) or Kruskal-Wallis test followed by non-parametric multiple comparisons test (#) reflecting differences between *Otof*$^{I515T/I515T}$and *Otof*$^{+/+}$ under different treatment conditions. Data from 2 mice and *n* ribbon synapses for each genotype/condition were analyzed.

Appendix Supplementary Methods

Mouse genetics

To generate *Otof*$^{I515T/I515T}$ mice, a targeting vector was constructed in which the codon coding for Ile515 (ATC) in exon 15 was replaced by a codon for threonine (ACA). The position 515 refers to the human protein sequence NP_001274418 and differs in the mouse protein sequence depending on the splice variant. In addition to the ATC to ACA replacement, a silent mutation was introduced 10 bp upstream of the new codon to introduce a KpnI restriction site for later screening. A neomycin selection cassette flanked by loxP sites was subcloned into the Pml1 restriction site in intron 15/16. The targeting construct consisted of 3- and 5.3-kb-long linkers for homologous recombination upstream of the point mutation and downstream of the loxP flanked neomycin cassette, respectively. A thymidine kinase cassette for negative selection was added after the 5.3-kb-long arm. This targeting construct was electroporated into 129ola embryonic stem cells, and cell colonies were picked after selection with G418 and ganciclovir. Homologous recombination was tested by Southern blot analysis after BclI digest using a BclI site upstream exon 11 and a newly introduced BclI site 5' of the neomycin cassette. Two clones were injected into mouse blastocysts, which both led to germ-line transmission in male chimeric mice. Heterozygous offspring from the chimeras were bred with an E2a cre-recombinase-expressing mouse line to excise the neomycin cassette. Mice were back-crossed with C57Bl6/N mice to out-breed the *Cre* recombinase.

For immunohistochemistry, cellular physiology and intellicage experiments, *Otof*$^{I515T/I515T}$ mice from a line that had been backcrossed for at least four generations with C57Bl6/N were used. For some experiments, *Otof*$^{I515T/I515T}$ mice were cross-bred with otoferlin knock-out mice (described in Reisinger *et al*, 2011). For single unit recordings and startle response measurements, we crossbred *Otof*$^{I515T/I515T}$ mice for five generations with CBA mice.

Immunohistochemistry and fluorescence imaging

Immunostaining was performed essentially as previously described (Khimich *et al*, 2005) with the following modifications: For acutely isolated organs of Corti at P14-P15, a major part of the bony shelf of the cochlea was removed and the round window was perforated to allow solutions to access the organ of Corti within the temporal bone. Fixation in 4% formaldehyde (FA) in PBS, blocking and antibody application was performed with the organ of Corti situated in the opened cochlea. Finally, the apical turn was excised from the cochlea and mounted in Moviol. For acute preparations at an age of 9-16 weeks, the temporal bone was locally perfused with 4% FA in PBS for 10 min, decalcified for 10 min in Morse's solution and the organ of Corti in the apical and basal turns were dissected. For incubations at different temperatures, organs of Corti at P7-P8 were excised from temporal bones in HEPES-buffered Hanks solution (Gibco) supplemented with 10µg/ml Penicillin G (Sigma-Aldrich) and 250 ng/ml Fungizone (Life Technologies). The tissue was then transferred to DMEM-F12 Glutamax 1 (1:1) medium (Life Technologies) with 5% fetal calf serum (Invitrogen) and mounted on coverslips coated with Cell-Tak™ (BD Biosciences). The organotypic cultures were allowed to settle for 24 hours and were then incubated at the indicated temperature.

For immunostainings, the following antibodies were used: mouse IgG1 anti-Ctbp2 (RRID:AB_399431, BD Biosciences, Heidelberg, Germany, 1:200), rabbit anti-GluR2 Clone 6C4 (RRID:AB_2113875, Chemicon/Merck Millipore, 1:200), mouse anti-otoferlin (RRID:AB_881807, Abcam, Cambridge, UK, 1:300), rabbit anti-otoferlin (Synaptic Systems, Göttingen, Germany, 1:300), rabbit anti-Vglut3 (RRID:AB_10015218, Synaptic Systems, 1:300), mouse anti-calbindin D28k (Swant, Switzerland, 1:1000) rabbit anti-sodium/potassium-ATPase α (Santa Cruz Biotechnology, Dallas, USA, 1:200), guinea pig anti-Parvalbumin (RRID:AB_1547406, Synaptic Systems, 1:200) and secondary Alexa Fluor®405, Alexa Fluor®488-, Alexa Fluor®568-, Alexa Fluor®594-, and AlexaFluor647-labeled antibodies (Invitrogen, 1:200). Confocal morphological images were acquired using a laser scanning confocal microscope (Leica TCS SP5, Leica Microsystems CMS GmbH, Mannheim, Germany) with a 63x Glycerol immersion objective (NA = 1.456) or a 100x oil immersion objective (NA = 1.3). Whole-mount preparations of the organ of Corti allowed analyzing several IHCs in a row (Khimich *et al*, 2005). For 3D reconstructions of the specimen, z-axis stacks of 2D images were taken with a step size of 0.5-0.8 µm. The number of synapses in 14-16 day old IHCs were counted using the cell counter plugin in *ImageJ* software as number of Ctbp2 spots adjacent to GluR2 spots. Synaptic ribbons in 9-16 week old animals were counted as Ctbp2-positive clusters within Parvalbumin-stained IHCs juxtaposed to NaK-ATPase-stained synaptic boutons using the ROI Manager plugin in *ImageJ*. Image analysis to determine fractional levels of membrane bound otoferlin is described in Figure 1. For analysis of organotypic cultures (Fig 6), the membrane position determined with the threshold method was always very close to the most basal peak value in subtracted fluorescence, which is why we took the maximum of the latter peak value for analysis. For IHCs after biolistic transfection (Fig 5), we used a threshold of 5 in summed fluorescence for quantification of the fractional membrane staining of otoferlin.

Patch clamp recordings

The pipette solutions for perforate-patch experiments contained (in mM): 130 Cs-gluconate, 10 Tetraethylammonium-chloride (TEA-Cl), 10 4-aminopyridine (4-AP, Merck, Darmstadt, Germany), 1 $MgCl_2$, 10 Cs-HEPES (pH adjusted to 7.17, osmolarity approx. 290 mOsm), 300 µg/ml amphotericin B (Calbiochem, La Jolla, CA). For flash photolysis of caged Ca^{2+} we recorded in ruptured patch condition with a pipette solution containing (in mM) 120 Cs-gluconate, 20 TEA-Cl, 20 Cs-HEPES (pH adjusted to 7.2), 0.3 mag-fura-2 (Invitrogen, Karlsruhe, Germany), 10 DM-nitrophen (gift of A. Leonov and C. Griesinger, Göttingen), 5 DPTA (1,3-diaminopropan-2-ol-tetraacetic acid) and 10 $CaCl_2$. The extracellular solutions contained (in mM): 113 NaCl, 35 TEA-Cl, 2.8 KCl, 2 $CaCl_2$ (10 for flash-photolysis), 1 $MgCl_2$, 10 Na-HEPES, 1 CsCl, 11.1 D-glucose (pH adjusted to 7.2, osmolarity approx. 300 mOsm). All chemicals were obtained from Sigma-Aldrich (Taufkirchen, Germany) unless stated otherwise. EPC-9 or EPC-10 amplifiers (HEKA Electronics, Lambrecht, Germany), controlled by *Pulse* or *Patchmaster* software, were used to sample and filter currents at 20 kHz and at 5 kHz, respectively. We measured ΔCm as previously described using depolarizations of different durations to peak Ca^{2+} current potential at intervals of 30 to 60 s (Beutner & Moser, 2001). All currents were leak-corrected using a P/6-protocol.

The vesicle replenishment rate was calculated as cell capacitance change during 100 ms depolarization minus the evoked release at 20 ms depolarization, divided by 45 aF per vesicle (Neef *et al*, 2007) to get the number of vesicles. Further, a number of 13 synapses per cell was used (Figure S4) to calculate the vesicle rate per active zone. This divided by 0.08 s gives the rate per second.

For $Otof^{+/+}$, ΔCm was 51.45 fF for 100 ms and 16.08 fF for 20 ms depolarization.

Replenishment rate = (51.45 fF – 16.08 fF)/0.045 fF/14 synapses/0.08s = 702 vesicles/s/active zone.

For $Otof^{I515T/I515T}$, ΔCm was 30.42 fF for 100 ms and 13.35 fF for 20 ms depolarization.

Replenishment rate = (30.42 fF-13.35 fF)/0.045 fF/14 synapses/0.08s = 339 vesicles/s/active zone.

Flash photolysis was performed as described (Beutner *et al*, 2001). If not otherwise indicated, recordings were performed at room temperature (20-25°C).

For recordings at elevated temperature, perforation solution and the objective lens were heated and the temperature was controlled by a miniature thermistor in ~1mm distance from the organ of Corti as described (Nouvian, 2007). Heating to 35-36.5°C took approximately 3-7 min. Recordings were started as soon as the temperature was at least 1 min between 35°C and 36.5°C. Similarly, recordings at higher temperature were performed as soon as the temperature was at 38.5-40°C.

Quantification of single unit responses

PSTHs were calculated as average spike rates using 200 presentations of 50ms tone bursts presented at CF, 30dB above threshold. Onset/peak rate was quantified as the largest bin of the PSTH (binwidth 0.5ms). Adapted rate was averaged in a window between 35 and 45ms following stimulus onset. Individual PSTHs were averaged after aligning for the time when they reached 30% of the difference between spontaneous and peak rate. Rate level functions were obtained using 50ms tone bursts presented at 5 Hz with 25 repetitions for each stimulus intensity. Threshold was interpolated from the rate level function as the intensity at which the spike rate increased by 20 Hz above spontaneous rate. The steepness was calculated as the increase in average spike rates for each 5 dB intensity increment. Dynamic range was calculated based on sigmoidal fits to the rate intensity function as described in (Taberner & Liberman, 2005). For analysis of forward masking data, spike numbers in a 5ms interval starting from response onset were determined and presented as the ratio of probe and masker responses for at least 25 repetitions for each interval. The adapted rate of the masker response was determined in a window 85-90ms following stimulus onset. The data was then normalized to 0 for the peak to adapted spike rate ratio and 1 for full recovery at the next masker onset. Then, the half time of recovery was determined from a logarithmic fit to the normalized recovery curve. For amplitude modulation analysis, the synchronization index, also called vector strength was calculated as described by (Goldberg & Brown, 1969). Synchronization indices were only considered significant when at least 15 spikes were present in a 3s recording interval and the Rayleigh statistic was below 13.8.

Startle responses

For measurements of startle responses, mice were placed in a custom-designed small cage on a mobile platform inside a sound-shielded box (Desone). To elicit startle responses, 12 kHz tone bursts or broadband white noise of 10 ms duration was administered at variable intensities using a high-frequency speaker system (ScanSpeak, Avisoft) mounted 15 cm above the cage. The minimal interval between two stimuli was randomly varied between 10 and 20 s. Stimuli were delayed by additional 5 s when mouse movements exceeded a manually set threshold during the pause. Stimulus generation and response recordings were performed using Tucker Davis System III and custom-written *Matlab* software. The summed integral output of accelerometers attached to the

cage in the x, y and z dimensions was analyzed in a time window of 9-20 ms following startle stimulus onset. For analysis of prepulse inhibition, 70 dB broadband noise was applied continuously, which was interrupted in 70 % of cases by a silent gap which preceded the startle stimulus (10 ms noise burst 115 dB) by 70 ms. Each stimulus condition was repeated at least 40 times in pseudorandom order. For analysis, we compared the distributions and median amplitudes of startle responses in the "no gap" condition with those of the different "gap" gap conditions and defined the gap detection threshold as the minimal gap duration which significantly reduced the startle response amplitude with all longer gaps also yielding a significant change (Mann-Whitney U test $p<0.007$, corresponding to a p value of 0.05 with Bonferroni correction for 7 comparisons).

Operant conditioning

Operant conditioning in the "Audiobox" was carried out essentially as described in (de Hoz & Nelken, 2014). Female mice were transponder-injected and habituated to the social cage environment which was enriched by houses and running wheels at an age of 4 weeks. During a habituation phase of at least 5 days, in which drinking was allowed at every visit in the sound-attenuated chamber while no sound (for threshold testing) or continuous 70 dB broadband noise (for gap detection) was played. We then introduced conditioned stimuli (80 dB 12 kHz tone bursts, 400 ms duration, 3 stimuli/second, or continuous 70 dB broadband noise interrupted by 3 90 ms gaps per second) in 5% of visits and punished drink attempts by air puffs to the back of the mouse, giving no water access. The fraction of conditioned stimuli was slowly increased to 20% over at least 3 weeks, depending on the discrimination performance of each mouse. In a subsequent generalization phase, the conditioned stimuli were varied in intensity (70-90 dB) or gap duration (70-90 ms), respectively. Finally, the experimental phase included rare interspersed stimuli of intermediate intensity or duration. Only data from mice that reached a discrimination performance of a difference of at least 0.3 between conditioned and unconditioned stimuli was used.

All loudspeaker systems were calibrated using a 1⁄4" microphone (D 4039, Bruel and Kjaer GmbH). For the Intellicage, an approximate average intensity detected in multiple locations within the corner with the water bottles was chosen for display.

Cloning of full length otoferlin

Full length otoferlin cDNA was subcloned from mouse organ of Corti cDNA by assembly of four fragments all amplified by PCR. The fragments were gained using oligonucleotides (all in 5'-3' direction) GAGAGAATTCGCCACCATGGCCCTGATTGTTCACCTC and CAGCAAAGAAGACTTGCACATAGG (1st fragment); GGTGAGAACAAGGACCTCGTC and GTGTCTCGTTTAGAACCTCAGTGC (2nd fragment); GCACTGAGGTTCTAAACGAGACAC and GGGTCCCTCCAGATATTGTAGC (3rd fragment), and CAGACCTATTCCATACATGGCTAC and GAGAGGTACCTCAGGCCCCTAGGAGCTT-CTTGACCATG (4th fragment). Fragments were assembled either with overlap PCR of with restriction enzyme cloning. Sanger Sequencing revealed a transcript variant that is now deposited under GeneBank accession No KX060996. The open reading frame sequence is congruent with reference sequence NM_001313767.1, termed otoferlin transcript variant 4.

Cloning of the RXR motif

By site-directed mutagenesis the human "RXR motif", comprising amino acids TVRLLRRCRVLCNGGSSSHS (amino acids 1244-1263 in NP_001274418) was subcloned into a pcDNA3 plasmid containing mouse otoferlin cDNA using overlap PCR. In addition, a site directed mutation for N1240S was included in the mouse sequence to mimic the human sequence (see Fig EV4). Oligonucleotides used were CGGCGCTGCCGTGTGCTGTGCAATGGGGGCTCCTCCTCTCACTCCACAGGGGAGGTTGTAGTAAGC (fwd) and CTCTTTACAGAGGCGTGTCAGG (rev) for one PCR and CAATGATTGACCGGAAAAA-TGGGG (fwd) and CACAGCACACGGCAGCGCCGGAGAAGCCTGACCGTGGTGTTCCAGCTGGGGGC-TGAGCGGTCTGG (rev) for the second PCR generating overlapping sequences including the codons for the inserted/mutated amino acids. The two amplicons were assembled by overlap PCR and sublconed into the original vector with SanDI and SfiI. The construct was verified by Sanger Sequencing, amplified and purified for biolistic transfection.

Gene Gun transfection of otoferlin deficient mouse organs of Corti

Gene Gun bullets were prepared according to the instructions of Woods and Zito (2008) with the following modifications: 25 mg gold with a diameter of 1 µm (Bio-Rad) were mixed with 100 µl 0.05M spermidine (Sigma-Aldrich), vortexed for 15 sec and sonified for 30 sec (Transsonic 820/H, Elma). 50 µg DNA (1 µg/µl) (90% pcDNA3-mOtof and 10% pEGFP-N1, w/w) in 50 µl H_2O were added to the solution and vortexed for 5 sec. 100 µl of 1 M $CaCl_2$ (Sigma-Aldrich) was added drop-wise to the mixture while vortexing. The mixture was incubated at RT for 10 min, while vortexing every 30 sec for 5 sec and centrifuged for 2 min (1000 g). Three wash (100% EtOH) and centrifugation steps (10 sec, 1000 g) followed. The mixture was resuspended in 3

ml Polyvinylpyrrolidone (PVP) (50 µg/ml) (Bio-Rad, USA) and vortexed for 15 sec. A 70-80 cm long Tefzel tubing (Bio-Rad) was dried using nitrogen (0.4 l/min) for at least 15 min in the tubing station (supplied with the Helios® Gene Gun System) and filled with the gold particle solution. The gold particles were distributed evenly inside the tubing piece as described in Woods and Zito, 2008. The tubing piece was left to dry by nitrogen flow (0.4 l/min, 5 min), cut into appropriate pieces using the supplied tubing chopper and stored desiccated at 4°C until further use.
For Gene Gun experiments, *Otof*$^{-/-}$ mice (Reisinger *et al*, 2011) at the age of P4 were used. The isolated organs were oriented with the basilar membrane facing upwards. The biolistic transfection was performed via the Helios® Gene Gun System (Bio-Rad, USA) with a pressure of 200-210 psi and a distance of 3.5 cm between the tissue and focusing nozzle. To reduce the amount of gold particles arriving at the tissue, two Falcon® 40 µm or 70 µm cell strainers (Corning, USA) were placed between the focusing nozzle and the sample (modified from Zhao *et al*, 2012). After biolistic transfection, medium with 1.5 µg/ml Ampicillin (Sigma-Aldrich) was added, then the stria vascularis was removed, and the organs were attached to the cover slips. The cultures were left to incubate for two days at 37°C before further experiments were conducted. EGFP fluorescence served to control for efficiency of transfection prior to immunohistochemistry. Cultures transfected with otoferlin RXR motif and Ile515Thr mutation were either incubated at 37°C or at 38.5°C for 30 min before fixation and immunostaining.

Pre-embedding immunogold labeling
Organs of Corti were isolated and immediately fixed on ice (4°C) for 35 minutes for saponin permeabilized (4 % PFA in PBS) and 90 minutes for Triton X-100 permeabilized samples (2 %PFA, 0.6% glutaraldehyde in 1X PEM solution (0.1 M PIPES, 2 mM EGTA, 1 mM $MgSO_4x7H_2O$)). For saponin permeabilization the samples were additionally incubated for 45 min in 0.05 % saponin (Carl Roth) diluted in PBS. Subsequently samples were blocked for 1 hour at RT in blocking solution (saponin permeabilization: 2 % BSA and 3 % NHS in PBS; Triton X-100 permeabilization: 2 % BSA, 3 % NHS, and 0.2 % TritonX-100 in PBS). The primary antibody incubation was performed overnight at 4°C after 1 hour incubation at RT. The secondary antibodies were applied to the samples for 2 hours at RT after three washing steps (saponin permeabilization: PBS; Triton X-100 permeabilization: 0.1 % TritonX-100 in PBS) and then left to wash again overnight at 4°C. The following primary antibodies were used; mouse anti-otoferlin antibody (N-terminal, Abcam, 1:300) in both pre-embedding protocols and rabbit anti-Vglut3 (Synaptic Systems, 1:300) in the Triton X-100 permeabilization protocol. As secondary antibodies the Nanogold® anti-mouse IgG antibody and the Nanogold® anti-rabbit IgG antibody (Bio Trend, Germany, 1:30) were used. All antibodies were diluted in PBS with 5% NHS for saponin permeabilized and PBS with 0.1% Triton X-100 for Triton X-100 permeabilized samples. The samples were washed once again afterwards for 30 min at RT, post-fixed for 30 min at RT with post-fixation solution (2% glutaraldehyde in PBS) and further washed four times at RT for 10 min in distilled water. The silver enhancement step was performed light protected for 2.5 min using the HQ Silver Enhancement kit (Nanoprobes, USA) according to the manufacturer's instructions. Four wash steps with distilled water at RT for 10 minutes followed. Next, samples were incubated in 2% OsO_4 (Sigma-Aldrich, USA) diluted in 0.1 M cacodylate buffer (pH 7.2) (Carl Roth, Germany) for 30 min, washed once for one hour and twice for 30 minutes in distilled water. After washing, several dehydration steps with ascending ethanol concentrations (5 min in 30% ethanol, 5 min in 50% ethanol, 10 min in 70% ethanol, two times for 10 min in 95% ethanol, and three times for 12 min in 100% ethanol) were performed. The organs of Corti were placed in a mixture of 100% ethanol and pure EPON (1:1) prepared from the EPON Agar 100-premix Kit (Plano, Germany) and incubated once for 30 minutes and once for 1.5 hours at RT. Subsequently, the solution was replaced by pure EPON and left to incubate once overnight and once for 6 hours. The polymerization of the samples was performed in pure EPON for two days at 70°C.

Conventional embedding for transmission electron microscopy
After stimulation or inhibition the samples were fixed immediately with 4% PFA and 0.5% glutaraldehyde. Samples were dehydrated, infiltrated and embedded in Epon resin as described previously (Wong *et al*, 2014). After embedding, 70 nm sections for 2D transmission electron microscopy and 250 nm sections for electron tomography were obtained on an Ultracut E ultramicrotome (Leica). Sections were applied to formvar-coated copper slot or mesh (tomography) grids and post-stained with 4% uranyl acetate and Reynold's lead citrate.

Electron tomography
10 nm gold particles (British Bio Cell) were applied to both sides of the stained mesh grids. Single tilt axis series were acquired at a JEOL JEM 2100 transmission electron microscope at 200 kV from -60 to +60 with 1° increment using the Serial-EM software. The tomograms were generated using the IMOD package etomo and models were rendered using 3dmod (*bio3d.colorado.edu/imod/*) as described (Wong *et al*, 2014; Vogl *et al*, 2015).

EM Image analysis

Quantitative image analysis for random ultrathin sections was done using the *ImageJ* software package. Two morphological vesicle pools at ribbon synapses were analyzed , (i) membrane proximal vesicles (≤25 nm vesicle-to-membrane distance to the active zone membrane) and (ii) ribbon associated vesicles defined as all vesicles in the first row in ≤80 nm distance around the ribbon (excluding membrane proximal vesicles; see also Figure 7O). For calculation of the vesicle diameter in random sections, the average of the longest and the shortest axis was calculated. Image analyses for the tomograms were performed in *3dmod* (*bio3d.colorado.edu/imod/*). For ribbon-associated synaptic vesicles the first row of vesicles with a maximal distance of 80 nm from the ribbon to the vesicle membrane were counted per tomogram. Membrane-proximal synaptic vesicles were defined as vesicles with a membrane-to-membrane distance to the active zone of maximal 50 nm (Figure 8E) (Jung *et al*, 2015). Vesicle diameters were measured at the maximum projection for the round synaptic vesicles and the longest axis for the flattened vesicles. The height of the ribbons was determined as the maximum extent from the presynaptic density in both ultrathin and virtual sections.

The diameter of the otoferlin labeled structures was measured as described for the vesicle diameter measurement above. The number of anti-otoferlin gold clusters was counted over the length of the basal plasma membrane and indicated as gold clusters/µm. For quantifying the gold cluster amount within the IHC basal region, the clusters were counted within areas from 0-800 nm and 800-1600 nm distant to the plasma membrane and indicated as gold clusters/μm^2.

Quantitative PCR

Apical and midbasal turns of P9 organs of Corti were dissected from three $Otof^{+/+}$ and two $Otof^{I515T/I515T}$ mice. Tissue was homogenized in Trizol reagent (Life Technologies) and RNA was extracted according to the Trizol protocol. Precipitated RNA was dissolved in 13 µl H_2O, and 0.4 µl random hexamers (biomers.net; 0.5 µg/µl), 0.65 µl oligo dT primers (50 pmol/µl) and 1.3 µl dNTPs (10 mM each) were added. After incubation at 65°C for 5 min and cooling to 4°C, 5.3 µl first strand buffer, DTT (final concentration 1 mM), 260 U SuperScript® II (Invitrogen/Life Technologies) and 50 U RNAseOUT (Life Technologies) were added. Reverse transcriptase reaction was incubated for 10 min at room temperature, 30 min at 37°C and 1h at 42°C. Resulting cDNA was ethanol precipitated in presence of 1µg Glycogen and dissolved in 25µl H_2O. Real Time PCR was performed using Taqman assays Mm00453306 (Applied Biosystems) for amplification of otoferlin, Mm00446873_m1 for tata binding protein (TBP) and Mm00464451_m1 for bassoon on 2 µl of cDNA solution each.

To average (logarithmic) C_t values from parallel experiments (same cDNA, same primers), first a linear value was calculated from C_t values by

$Lin(C_t) = 2\text{^}(42-C_t)$

assuming that a single cDNA molecule would result in a C_t of 42 (any deviations from this value would not change the overall result, as this is eliminated in the next step).

$Lin(C_t)$ values were averaged, and back-calculated into "real" C_t values by

$C_t = 42 - LN(Lin(C_t))/LN2$

(Here the value of 42 is eliminated again, thus any other value could be assumed instead of the 42).

These averaged C_t values were then used to calculate ΔC_t values for each cDNA sample by

$\Delta Ct = C_t(Otof) - C_t(TBP)$.

Also, ΔC_t values from the individual cDNA preparations were averaged by calculating a linear value ΔC_t first which was averaged and back-calculated, as described for the C_t values. Relative mRNA amount (equivalent to cDNA amount) in mutant vs wt cDNA is then calculated by

$\Delta\Delta Ct = \Delta C_t$ (mutant) $- \Delta C_t$ (wt)

Relative Otof mRNA amount = $2\text{^}-\Delta\Delta C_t$.

HEK cell transfection and mass spectrometric quantification of otoferlin levels

Otoferlin cDNA (KX060996) was subcloned into pEGFP-N1 with a STOP codon such that no eGFP was transcribed from this plasmid. Mutations were introduced with overlap PCR and confirmed by Sanger sequencing. HEK293T cells between passages p3 up to p30 were used for experiments. Cells were transfected with desired plasmid DNA using Lipofectamine 2000 (Invitrogen / Life Technologies) according to the manufacturer's instructions and incubated overnight.

After 24h, 100 µg/ml cycloheximide was added to the cells and cells were incubated either at 37°C or at 38.5°C. Samples were taken at 0 min (control without cycloheximide), 5 min, 10 min, 20 min, 30 min, 60 min and 120 min, dissolved in 100 µl Laemmli Sample Buffer each (50 mM Tris pH 6.8, 20% SDS, 0.1% Bromophenol Blue, 10% glycerine, 100 µM DTT) and stored at -20°C until the last sample was taken. Samples were then thawed, sonified (3x20sec, Branson Sonifer 250) and 20 µl of each sample was loaded on an SDS PAGE consisting of 4% stacking gel and 6% running gel. The gel was stained in Coomassie Blue solution (10% acetic acid, 47.5% ethanol, 0.25% Coomassie Brilliant BlueR250) and destained in H_2O. Gel slices in the range of otoferlin size were cut out, washed, reduced with dithiothreitol (DTT), alkylated with 2-iodoacetamide and

digested with trypsin overnight. The resulting peptide mixtures were then extracted, dried in a SpeedVac, reconstituted in 2% acetonitrile/0.1% formic acid/ (v:v) and analyzed by nanoLC-MS/MS as described previously (Atanassov & Urlaub, 2013).
For mass spectrometric analysis samples were enriched on a self-packed reversed phase-C18 precolumn (0.15 mm ID x 20 mm, Reprosil-Pur120 C18-AQ 5 µm, Dr. Maisch, Ammerbuch-Entringen, Germany) and separated on an analytical reversed phase-C18 column (0.075 mm ID x 200 mm Picofrit 360-20-10-N, New Objective, Woburn/MA, USA, packed with Reprosil-Pur 120 C18-AQ, 3 µm) using a 37 min linear gradient of 5-35 % acetonitrile/0.1% formic acid (v:v) at 300 nl min^{-1}). The eluent was analyzed on a Q Exactive hybrid quadrupole/orbitrap mass spectrometer (ThermoFisher Scientific, Bremen) equipped with a FlexIon nanoSpray source and operated under Excalibur 2.2 software using a data-dependent acquisition method. Each experimental cycle was of the following form: one full MS scan across the 350-1600 *m/z* range was acquired at a resolution setting of 70,000 FWHM, a target of $10e^6$ and a maximum fill time of 60 ms to select up to ten most abundant peptide precursors of charge states 2 to 5 above a $10e^4$ intensity threshold, at an isolation width of 2.0 *m/z*. Precursors were fragmented by Higher Collision Energy Dissociation (HCD) with nitrogen at a normalized collision energy setting of 25%, and their product ion spectra recorded using a start mass of 100 *m/z*, a resolution setting of 17,500 FWHM (full width, half maximum), a target of $2x10e^5$ and a maximum fill time of 60 ms. Selected precursor *m/z* values were then excluded for the following 15 s. Three technical replicates per sample were acquired.
The MS raw files were processed by MaxQuant (Cox & Mann, 2008) (version 1.5.2.8) and MS/MS spectra were searched against mouse database (UniProt, downloaded July 2014; 51,547 entries) supplemented with 245 frequently observed contaminants via the Andromeda search engine (Cox *et al*, 2011). Mass tolerance after recalibration of precursor mass and fragment ion mass were set as 6 and 20 ppm, respectively. Allowed variable modifications included protein N-terminal acetylation and methionine oxidation. Cysteine carbamidomethylation was defined as a fixed modification. Minimal peptide length was set to 7 amino acids with the maximum of two enzymatic mis-cleavages. The false discovery rate (FDR) was set to 1% for both peptide and protein identifications. For relative quantitation, intensities of all identified peptides were determined by the MaxQuant with the option of "match between runs" on. Intensity-based absolute quantification or iBAQ values (Schwanhäusser *et al*, 2011) of all identified proteins were then calculated to represent their quantity in the sample.

In order to eliminate possible system variations introduced during sample handling and during mass spectrometric analysis, we normalized the iBAQ value of otoferlin against that of stable background proteins, which were defined as those proteins showed most reproducible iBAQ values with relatively high abundance across all replicates. We carefully examined the abundance and iBAQ variations of all identified proteins over biological and technical replicates. To this end, four protein hits with the leading gene names as Spag9, Top2b, Brd4, and Uba52 were selected for following normalization.

Supplementary References

Atanassov I & Urlaub H (2013) Increased proteome coverage by combining PAGE and peptide isoelectric focusing: comparative study of gel-based separation approaches. *Proteomics* **13:** 2947–2955

Beutner D & Moser T (2001) The presynaptic function of mouse cochlear inner hair cells during development of hearing. *J Neurosci* **21:** 4593

Beutner D, Voets T, Neher E & Moser T (2001) Calcium dependence of exocytosis and endocytosis at the cochlear inner hair cell afferent synapse. *Neuron* **29:** 681–690

Cox J & Mann M (2008) MaxQuant enables high peptide identification rates, individualized p.p.b.-range mass accuracies and proteome-wide protein quantification. *Nature biotechnology* **26:** 1367–1372

Cox J, Neuhauser N, Michalski A, Scheltema RA, Olsen J V. & Mann M (2011) Andromeda: A peptide search engine integrated into the MaxQuant environment. *Journal of Proteome Research* **10:** 1794–1805

Goldberg JM & Brown PB (1969) Response of binaural neurons of dog superior olivary complex to dichotic tonal stimuli: some physiological mechanisms of sound localization. *J. Neurophysiol.* **32:** 613–636

de Hoz L & Nelken I (2014) Frequency tuning in the behaving mouse: different bandwidths for discrimination and generalization. *PLoS ONE* **9:** e91676

Jung S, Maritzen T, Wichmann C, Jing Z, Neef A, Revelo NH, Al-Moyed H, Meese S, Wojcik SM, Panou I, Bulut H, Schu P, Ficner R, Reisinger E, Rizzoli SO, Neef J, Strenzke N, Haucke V & Moser T (2015) Disruption of adaptor protein 2μ (AP-2μ) in cochlear hair cells impairs vesicle reloading of synaptic release sites and hearing. *EMBO J.* **34:** 2686–2702

Khimich D, Nouvian R, Pujol R, tom Dieck S, Egner A, Gundelfinger ED & Moser T (2005) Hair cell synaptic ribbons are essential for synchronous auditory signalling. *Nature* **434:** 889–894

Marlin S, Feldmann D, Nguyen Y, Rouillon I, Loundon N, Jonard L, Bonnet C, Couderc R, Garabedian EN, Petit C & Denoyelle F (2010) Temperature-sensitive auditory neuropathy associated with an otoferlin mutation: Deafening fever! *Biochem. Biophys. Res. Commun* **394:** 737–742

Matsunaga T, Mutai H, Kunishima S, Namba K, Morimoto N, Shinjo Y, Arimoto Y, Kataoka Y, Shintani T, Morita N, Sugiuchi T, Masuda S, Nakano A, Taiji H & Kaga K (2012) A prevalent founder mutation and genotype–phenotype correlations of OTOF in Japanese patients with auditory neuropathy. *Clinical Genetics* n/a–n/a

Neef A, Khimich D, Pirih P, Riedel D, Wolf F & Moser T (2007) Probing the mechanism of exocytosis at the hair cell ribbon synapse. *The Journal of Neuroscience* **27:** 12933–12944

Nouvian R (2007) Temperature enhances exocytosis efficiency at the mouse inner hair cell ribbon synapse. *The Journal of Physiology* **584:** 535–542

Raman S, Vernon R, Thompson J, Tyka M, Sadreyev R, Pei J, Kim D, Kellogg E, DiMaio F, Lange O, Kinch L, Sheffler W, Kim B-H, Das R, Grishin NV & Baker D (2009) Structure prediction for CASP8 with all-atom refinement using Rosetta. *Proteins* **77 Suppl 9:** 89–99

Reisinger E, Bresee C, Neef J, Nair R, Reuter K, Bulankina A, Nouvian R, Koch M, Bückers J, Kastrup L, Roux I, Petit C, Hell SW, Brose N, Rhee J-S, Kügler S, Brigande JV & Moser T (2011) Probing the functional equivalence of otoferlin and synaptotagmin 1 in exocytosis. *J. Neurosci.* **31:** 4886–4895

Robertson NG, Khetarpal U, Gutiérrez-Espeleta GA, Bieber FR & Morton CC (1994) Isolation of novel and known genes from a human fetal cochlear cDNA library using subtractive hybridization and differential screening. *Genomics* **23:** 42–50

Romanos J, Kimura L, Fávero ML, Izarra FAR, de Mello Auricchio MTB, Batissoco AC, Lezirovitz K, Abreu-Silva RS & Mingroni-Netto RC (2009) Novel OTOF mutations in Brazilian patients with auditory neuropathy. *J. Hum. Genet* **54:** 382–385

Schwanhäusser B, Busse D, Li N, Dittmar G, Schuchhardt J, Wolf J, Chen W & Selbach M (2011) Global quantification of mammalian gene expression control. *Nature* **473:** 337–342

Söding J, Biegert A & Lupas AN (2005) The HHpred interactive server for protein homology detection and structure prediction. *Nucleic Acids Res.* **33:** W244-248

Taberner AM & Liberman MC (2005) Response Properties of Single Auditory Nerve Fibers in the Mouse. *J Neurophysiol* **93:** 557–569

Varga R, Avenarius MR, Kelley PM, Keats BJ, Berlin CI, Hood LJ, Morlet TG, Brashears SM, Starr A, Cohn ES, Smith RJH & Kimberling WJ (2006) OTOF mutations revealed by genetic analysis of hearing loss families including a potential temperature sensitive auditory neuropathy allele. *J Med Genet* **43:** 576–581

Vogl C, Cooper BH, Neef J, Wojcik SM, Reim K, Reisinger E, Brose N, Rhee J-S, Moser T & Wichmann C (2015) Unconventional molecular regulation of synaptic vesicle replenishment in cochlear inner hair cells. *J. Cell. Sci.* **128:** 638–644

Wang D-Y, Wang Y-C, Weil D, Zhao Y-L, Rao S-Q, Zong L, Ji Y-B, Liu Q, Li J-Q, Yang H-M, Shen Y, Benedict-Alderfer C, Zheng Q-Y, Petit C & Wang Q-J (2010) Screening mutations of OTOF gene in

Chinese patients with auditory neuropathy, including a familial case of temperature-sensitive auditory neuropathy. *BMC Med. Genet* **11:** 79

Wong AB, Rutherford MA, Gabrielaitis M, Pangršič T, Göttfert F, Frank T, Michanski S, Hell S, Wolf F, Wichmann C & Moser T (2014) Developmental refinement of hair cell synapses tightens the coupling of Ca2+ influx to exocytosis. *EMBO J* **33:** 247–264

Woods G & Zito K (2008) Preparation of gene gun bullets and biolistic transfection of neurons in slice culture. *J Vis Exp*

Zhao H, Avenarius MR & Gillespie PG (2012) Improved Biolistic Transfection of Hair Cells. *PLoS One* **7** Available at: http://www.ncbi.nlm.nih.gov/pmc/articles/PMC3462194/ [Accessed December 14, 2012]